HHS Public Access

Author manuscript

Acad Radiol. Author manuscript; available in PMC 2017 September 01.

Published in final edited form as:

Acad Radiol. 2016 September ; 23(9): 1137–1144. doi:10.1016/j.acra.2016.04.008.

Ultrafast bilateral DCE-MRI of the breast with conventional Fourier sampling: preliminary evaluation of semi-quantitative analysis

Federico D. Pineda, Ph.D., **Milica Medved, Ph.D.**, **Shiyang Wang, Ph.D.**, **Xiaobing Fan, Ph.D.**, **David V. Schacht, M.D.**, **Charlene Sennett, M.D.**, **Aytekin Oto, M.D.**, **Gillian M. Newstead, M.D.**, **Hiroyuki Abe, M.D. Ph.D.**, and **Gregory S. Karczmar, Ph.D.***

[a]Department of Radiology, University of Chicago, Chicago, IL, USA

Abstract

Rationale and objectives—To evaluate the feasibility and advantages of a combined high temporal/high spatial resolution protocol for DCE-MRI of the breast.

Materials and methods—Twenty-three patients with enhancing lesions were imaged at 3T. The acquisition protocol consisted of a series of bilateral, fat-suppressed 'ultrafast' acquisitions, with 6.9-9.9 s temporal resolution, for the first minute following contrast injection; followed by four high spatial resolution acquisitions with 60–79.5 s temporal resolution. All images were acquired with standard uniform Fourier sampling. A filtering method was developed to reduce noise and detect significant enhancement in the high temporal resolution images. Time-of-arrival (TOA) was defined as the time at which each voxel first satisfied all the filter conditions, relative to the time of initial arterial enhancement.

Results—Ultrafast images improved visualization of the vasculature feeding and draining lesions. A small percentage of the entire field-of-view (<6%) enhanced significantly in the 30 s following contrast injection. Lesion conspicuity was highest in early ultrafast images, especially in cases with marked parenchymal enhancement. While the sample size was relatively small, the average TOA for malignant lesions was significantly shorter than the TOA for benign lesions. Significant differences were also measured in other parameters descriptive of early contrast media uptake kinetics ($p<0.05$).

Conclusions—Ultrafast imaging in the first minute of breast DCE-MRI has the potential to add valuable information regarding early contrast dynamics. Ultrafast imaging could allow radiologists to confidently identify lesions in the presence of marked background parenchymal enhancement.

Keywords

DCEMRI; breast imaging; lesion kinetics; high temporal resolution

*Corresponding Author Department of Radiology, MC2026, The University of Chicago, 5841 South Maryland Avenue, Chicago, IL, USA 60637. Voice: (773) 702-0214, FAX: (773) 702-0371, gskarczm@uchicago.edu.

Introduction

Dynamic contrast-enhanced MRI (DCE-MRI) of the breast is a valuable tool for the detection and diagnosis of breast cancer (1). The kinetics of contrast media uptake and washout yield important markers for malignancy (2, 3). Typically, malignant tumors exhibit fast uptake of contrast media followed by washout in the delayed phase (2). Standard clinical contrast enhanced scans are generally performed with high spatial resolution to enable morphological evaluation of lesions and detect small cancers (4). The high spatial resolution required, combined with the large fields-of-view necessary to acquire bilateral images, leads to low temporal resolution, typically in the range of 60 to 75 seconds. As a result, important kinetic information is obscured.

Acquiring DCE-MRI with high temporal resolution is important, as it allows accurate classification of contrast media dynamics in suspicious lesions, and thus has the potential to aid discrimination between malignant and benign lesions. In addition, high temporal resolution allows accurate measurement of the arterial input function (AIF) for each patient, a critical step in quantitative pharmacokinetic analysis (5–7). However, the early events in contrast media uptake in normal breast and breast lesions have not been well characterized; thus it is difficult to know what temporal resolution is optimal for breast MRI.

Jansen et al., Pinker et al., and Planey et al. used conventional Fourier sampling methods to image contrast media uptake in the breast at high temporal resolution (8–10). Improvements in temporal resolution in these studies came at the expense of either greatly reduced coverage, or lower spatial resolution than standard clinical scans (e.g. Pinker et al. reduced spatial resolution from 1 mm to 1.7 mm isotropic voxels (10)). Nevertheless, these studies showed advantages in conspicuity of pre-invasive lesions, and estimation of pharmacokinetic parameters compared to standard, low temporal resolution, clinical scans.

The goal of this study was to characterize the kinetics of early enhancement in arteries, veins, malignant lesions, benign lesions, and normal-appearing parenchyma; and to evaluate the performance of parameters descriptive of early kinetics in differentiating malignant versus benign lesions. Potential advantages in lesion detectability were also investigated in this study. The protocol used conventional Fourier sampling to allow robust quantitative analysis, and a novel filtering and analysis method to identify rapidly enhancing lesions. The acquisition protocol used here can be easily implemented in a clinical setting, regardless of vendor or scanner type.

Images were acquired at lower spatial resolution, and relatively high SENSE acceleration factors during the first minute post contrast injection, to produce full bilateral, fat-suppressed breast images with temporal resolution ranging between 6.2 seconds and 9.9 seconds. Following an initial 60 seconds of fast imaging, subsequent images were acquired using a standard clinical protocol with high spatial resolution, intermediate SENSE factors, and low temporal resolution. The ultrafast images during the first minute after contrast media injection provide detailed information regarding the early kinetics in the breast, while later high spatial resolution acquisitions allow assessment of the morphology of small lesions. The results provide new information regarding contrast media uptake during the first minute

after injection, and demonstrate the potential diagnostic utility of high temporal resolution imaging. In addition, these results are useful for evaluating acceleration methods, and suggest new approaches to fast data acquisition and quantitative analysis.

Materials and Methods

Patient recruitment

Twenty three patients, with biopsy proven lesions or lesions detected on prior imaging studies, were recruited under an Institutional Review Board approved and Health Insurance Portability and Accountability Act compliant prospective study after obtaining informed consent. Inclusion criteria were the identification of enhancing lesions in the DCE-MRI series, available pathology results, or identification of stable benign enhancement compared to prior imaging studies. Images from 3 patients were excluded from the study, one due to failure to identify any residual enhancement post-biopsy, another because no pathology results were available, and one due to technical issues with fat-suppression. In total, 18 distinct malignant masses or areas of enhancement were imaged (primary and satellite lesions), as well as 15 benign findings. Malignant lesions imaged included: 8 primary invasive ductal carcinomas (IDC), 4 satellite IDC's, 4 ductal carcinomas in situ (DCIS), 1 metaplastic carcinoma, and Paget's disease. Median patient age was 43 years, with a range of 23 to 73 years. Benign lesions imaged were: three fibroadenomas, a complex sclerosing lesion, focal adenosis, papilloma, benign enhancing focus, enhancing skin lesion, usual ductal hyperplasia, ruptured duct, atypical ductal hyperplasia, lobular carcinoma in situ (LCIS), fibrotic stroma and focal scar.

MRI acquisitions

DCE-MRI studies were performed on a Philips Achieva 3T-TX scanner (Philips Healthcare, Best, The Netherlands) using a 16-channel bilateral breast coil (MammoTrak, Philips Healthcare). The acquisition parameters for the 'ultrafast' and standard clinical acquisition are summarized in Table 1. All images were acquired in the axial plane. Temporal resolution for fast scans ranged from 7 to 10 seconds, depending on the size of the field-of-view and number of slices acquired. The DCE series consisted of 1 standard clinical acquisition and 5 ultrafast acquisitions pre-injection, followed by 8 fast acquisitions (starting immediately after injection and ending 55 – 80 s after injection) followed by 4 standard clinical acquisitions after the injection of contrast media at a dose of 0.1 mM/kg gadobenate dimeglumine (Multihance, Bracco, NJ) at 2 ml/s, followed by a saline flush of 20 ml at 2 ml/s. The 5 ultrafast pre-contrast sequences were acquired to measure the noise level pre-contrast. Ultrafast and standard clinical acquisitions were acquired as one sequence block.

Data analysis

Data processing was performed with in-house software written in Matlab (MathWorks, Natick, MA). Ultrafast subtraction images were calculated by subtracting the average of the 5 pre-contrast (baseline) images from each of the eight post-contrast acquisitions. 'Enhancement gradient' images were also calculated from the difference between each post contrast image and the immediately preceding image. Maximum intensity projections (MIPs) were generated for the standard subtraction images and enhancement gradient

images to visualize the entire volume at each time-point. Arterial enhancement can easily be visualized in the MIPs, identifying the time-point at which the contrast media reaches the breast. Thus, lesion enhancement was measured relative to the time-of-arrival (TOA) of the contrast bolus in the mammary arteries, rather than the time of injection.

A digital filter was used to identify significantly enhancing voxels, and to reduce spurious enhancement due to noise or artifacts. The first condition of the filter was that the signal increase in a given voxel was greater than five times the standard deviation of the baseline signal in that voxel, measured from the five pre-contrast acquisitions. The value of 5 times the standard deviation was arrived at empirically, as it provided an adequate level of noise reduction. The second condition was that the signal enhancement was greater than 20% of the baseline signal. The final condition was that a voxel was required to satisfy the previous two conditions for at least two consecutive time-points. Time-of-arrival maps were created by color coding the time at which each voxel first satisfied the filter's first two conditions, relative to the time of initial arterial enhancement. These color maps where then overlaid on the higher spatial resolution standard clinical images.

Regions-of-interest (ROIs) were drawn around the lesions, on ultrafast and standard clinical images (at each time-point), under radiologists' guidance, and average signal enhancement was measured at each time-point. Background parenchymal enhancement (BPE) was measured for all cases by manually segmenting the parenchyma in a slice in the central part of the breast without any lesions present, and measuring the average signal intensity at each time-point. The signal intensity in the blood vessels feeding the lesions was also measured for each time-point. Percent signal enhancement (PSE) versus time data were fit to a truncated (uptake only) empirical mathematical model (EMM) for malignant lesions, benign lesions, and parenchyma, for only the high temporal resolution time-points (11–13):

$$PSE\,(t) = A\,(1 - \exp\,(-\alpha t))\,, \quad (1)$$

where A is the upper limit of percent enhancement, and α is the uptake rate (sec^{-1}). A truncated EMM was used to evaluate the potential diagnostic value of early kinetic data as measured with the proposed protocol. From the EMM parameters, three secondary parameters were calculated: initial area under the contrast enhancement vs. time curve (iAUC) (14), time to 90% of maximum enhancement (T90) and initial slope (defined as the product of the uptake rate and the upper limit of enhancement). T90 was used as a surrogate for time-to-peak enhancement.

The EMM was also used to refine the estimate of lesion TOA, as the model can be used to better pinpoint the time at which lesion signal enhancement was 20%, removing some of the dependence on the timing and temporal resolution of the sequence. Interpolation was also used to improve estimates of arterial TOA, linear interpolation was used between the two time-points before and after arterial enhancement reached 20%, and the point at which enhancement equaled 20% was estimated.

Lesion conspicuity was quantified by calculating the ratio of signal increase in the lesion to the signal increase of normal parenchyma at each time-point:

$$r(t) = \frac{(S(t) - S_0)_{lesion}}{(S(t) - S_0)_{parenchyma}}. \quad (2)$$

Statistical significance of differences in parameters that describe early kinetics, between malignant and benign lesions, was evaluated with Wilcoxon rank sum tests or z-test for proportions, where appropriate. Because multiple parameters were investigated Bonferroni corrections were used to correct for multiple comparisons.

Results

MIPs from ultrafast DCE-MRI (Figure 1, a-d standard subtractions, g-h enhancement gradient) show signal increase in the vessels, including very early enhancement in tortuous vessels directly feeding tumors, followed by signal increase in the tumors. The enhancement gradient images show a slowing signal increase in the arteries, and in Figure 1g a blood vessel posterior and lateral to the lesions is seen enhancing immediately after enhancement of the lesion; this is likely a vein draining the tumor. For most cases (19 out of 20), significant arterial enhancement (> 20%) was measured in the second or third ultrafast post-contrast image, in the internal mammary artery. For three cases, the vessel feeding the lesion began to enhance at the same time as the internal mammary artery. In all other cases, the vessel feeding the lesion enhanced later than the internal mammary artery.

The average percentage of voxels in the whole field-of-view (FOV) satisfying the filter conditions started at 0.4% of the FOV at the first time-point post injection (when in most cases only the heart was enhanced) and monotonically rose to 5.7% ± 1.9% at the 4^{th} time-point, and 7.3% ± 2.5% of the entire FOV by the last ultrafast acquisition.

Time-of-arrival (TOA) maps were created as a way of visualizing the time at which lesions began enhancing and heterogeneity of the time of initial enhancement within lesions. Examples of these maps can be seen in Figure 2, for both malignant and benign lesions. The results shown are typical of the lesions imaged; the average TOA was much shorter ($p < 0.01$) for malignant lesions (18.4 s ± 12.9 s) than for benign lesions (43.5 s ± 36.1 s). Intra-lesion heterogeneity in TOA can also be appreciated in these maps. In benign ROIs the average intra-lesion coefficient of variation in TOA was 0.58 ± 0.37, and in malignant lesions 0.38 ± 0.51.

Average signal enhancement from the ROIs, as a function of time, is plotted in Figure 3 for malignancies (n = 18), benign findings (n = 15) and BPE (n = 20). In this plot, percent signal enhancement is plotted relative to the time of injection. While there is a large spread in the percent signal enhancement of all lesions, on average malignancies were more strongly enhanced throughout the first minute than benign lesions and parenchyma, while parenchyma was least enhanced. The average EMM fits (using the parameters from Table 2) to the data from malignant lesions, benign lesions, and parenchyma are also plotted as solid

lines, using the average value of arterial time-of-arrival, 11.6 s ± 5.8 s relative to the injection time, for illustration purposes. The average values of the primary and secondary EMM parameters for benign and malignant lesions can be seen in Table 2. Significant differences (post-Bonferroni corrections) were found between benign and malignant lesions for all parameters except for 'A', the upper limit of enhancement. Times-of-arrival measured with the EMM parameters were shorter than those from direct measurement with the filter, due to better estimation of the time at which signal enhancement was 20% in both arteries and lesions.

Lesion conspicuity was measured as described in Equation 2. On average (across all lesions) this ratio was at its highest during the early ultrafast acquisitions, and reached its peak in the 4th ultrafast acquisition post-injection); where its average was 11:1, compared to 4.4:1 by the final (8th) ultrafast acquisition. The difference between ultrafast and conventional acquisitions was most pronounced in cases with marked BPE. Plots of the ratio of lesion signal increase to parenchymal signal increase can be seen in Figure 4, for three lesions in cases with marked BPE, in pre-menopausal women. In this figure, the vertical line indicates the time at which the standard clinical protocol would be acquiring the center of k-space ('k0'). For all of these cases the maximum conspicuity of the lesion occurs before the time to 'k0' in the standard clinical protocol. As a result, the conspicuity of these lesions would have been reduced on conventional clinical images, compared to images acquired with the ultrafast protocol. Subtraction images for three ultrafast time-points and the first time-point of the standard clinical protocol, from two of the cases (a fibroadenoma and a satellite IDC) can be seen in Figure 5.

Discussion

The data reported here add substantially to the relatively limited experience with ultrafast imaging of the breast using conventional, uniform Fourier sampling. A filter was developed to detect significant early enhancement, and the kinetic data were analyzed using a new quantitative method. The results suggest new approaches to data acquisition and analysis of ultrafast DCE MRI.

Ultrafast imaging resolved the early kinetics of lesions, blood vessels, and parenchyma in the first seconds after the contrast media bolus arrived in the arteries of the breast. On average, malignant lesions enhanced earlier and more rapidly than benign lesions. Ultrafast imaging allowed us to analyze the TOA data with respect to the time of initial arterial enhancement; this is not possible in conventional DCE-MRI with temporal resolution above one minute. As a result, ultrafast imaging allows evaluation of the local vasculature characteristics while reducing the influence of global variables such as cardiac output. In contrast, in standard clinical protocols, the enhancement in early images is dependent on when the contrast bolus reaches the breast, and thus on cardiac output which has significant intra- and inter-patient variability.

Time-of-arrival maps showed lesions clearly based on time of initial enhancement, and also showed heterogeneous enhancement of lesions at early times after injections. This information is not available from conventional clinical DCE-MRI and may help to increase

diagnostic accuracy and efficiency of radiologists. Although these preliminary results are by no means definitive – they suggest that ultrafast imaging provides novel information concerning contrast media dynamics at early times after injection, and this information may be clinically useful.

The current results also suggest that ultrafast imaging may detect early enhancement of lesions that occurs before parenchymal enhancement, thus making lesions more conspicuous; this is especially useful in cases with marked parenchymal enhancement (i.e. younger women) (15–17). This is consistent with previous results with high temporal resolution imaging from Jansen et al. (9), who sampled a limited number of slices with 7 second resolution and demonstrated that this approach detects significant differences between the early enhancement of DCIS and normal parenchyma, thus improving conspicuity of small diffuse cancers. Initial experience reported by Pinker et al. showed that a similar combined high temporal and high spatial resolution protocol allowed accurate detection and assessment of breast lesions, with a sensitivity of 100% and specificity of 72.2% (10). In addition to potentially increased sensitivity, ultrafast imaging may also improve specificity by ruling out cancer in cases where there is no significant lesion enhancement at early times after arrival of the contrast bolus in the breast.

The average TOA for malignant lesions measured here suggests significant enhancement begins shortly after arterial enhancement in the breast. A larger clinical trial is needed to determine an adequate cutoff for TOA between malignant and benign lesions. Refined TOA, estimated from the EMM parameters and linear interpolation of arterial enhancement, provided better estimates of the time at which enhancement actually reached the 20% threshold, at the cost of increased processing time (making this approach less practical in the clinic). In the present work, EMM fits were ROI based. Voxel-by-voxel fitting to the EMM would allow the creation of better TOA maps. However increased noise in these fits, and motion artifacts could affect the results.

The differences in average values of some of the kinetic parameters between benign and malignant lesions were very large, suggesting a large dynamic range for parameters derived from ultrafast data. For example, while the standard deviation was relatively large, initial slope differed by more than a factor of six between benign and malignant lesions. The mean uptake rate of malignant lesions was 5.2 times that of benign lesions. These differences are much larger than those reported for pharmacokinetic parameters such as K^{trans} (the volume transfer constant) (18). However, the number of lesions analyzed here was relatively small and a larger study will be necessary to confirm these results. A larger dataset will also allow for the testing of other kinetic parameters, or perhaps combinations of the parameters shown here. Receiver operating characteristic (ROC) analysis with a larger number of cases would determine which parameters (or combinations of parameters) perform best in a classification task (i.e. benign vs. malignant).

The results presented here, along with the results of previous studies (8–10, 19, 20), suggest the clinical benefits of ultrafast imaging of early contrast media kinetics. Recently Kuhl et al demonstrated the value of an abbreviated DCE-MRI protocol for breast cancer screening (21). Addition of ultrafast imaging to the abbreviated protocol could aid in the detection and

classification of lesions, without significantly increasing scan time. MIPs of subtraction and enhancement gradient images, as well as TOA maps, as proposed here, could provide a time-efficient method for the evaluation of early kinetics by radiologists.

The current ‘ultrafast’ images were acquired with only modest spatial resolution in order to increase temporal resolution. However, the very sparse early enhancement suggests that both high temporal and high spatial resolution could be achieved simply by allowing fold-back of early post-injection data into a smaller FOV, with post-processing to unfold images.

A number of methods have been used to acquire high temporal resolution scans. Many have focused on view-sharing or sliding window reconstruction techniques (e.g. DISCO, TWIST, TRICKS, 4D-TRAK) (22–29), where the center of k-space is sampled more frequently than the periphery and k-space data from a few acquisitions are combined to obtain higher spatial resolution. Mann et al. (19) implemented a variable spatiotemporal protocol using the TWIST technique for the ultrafast images, achieving a temporal resolution of 4.3 s for the initial part of the DCE series. They found that all the lesions imaged were visible on both the ultrafast and standard images, and that the maximum slope of the kinetic curve performed well in classifying lesion (area under the ROC curve = 0.829). These results are consistent with our finding that the initial slope was significantly different between benign and malignant lesions. A study by Platel et al. (20) using the TWIST protocol found that adding morphological information to the kinetic parameters increased the classification accuracy, and performed better than similar analysis in the low temporal resolution data. Platel et al. found that of the kinetic parameters time to maximum slope performed well (alone) in discriminating benign and malignant lesions (Az = 0.73). This parameter is likely related to the TOA parameter analyzed in this study, confirming that determining the time and rate at which lesions begin to enhance may have significant clinical importance. While these approaches generate excellent images, and capture the initial rate of signal enhancement in lesions, sampling outer portions of k-space at relatively low temporal resolution makes it difficult to interpret kinetics of enhancement, especially for small features with high spatial frequency components. Compressed sensing (CS) approaches have also been proposed as an alternative for accelerating DCE-MRI without significant sacrifices in spatial resolution (30–33). Specifically, for breast imaging, a reference image based compressed sensing (RICS) technique has been tested and shown to be feasible for clinical breast DCE-MRI. However, CS is susceptible to artifacts, particularly when enhancement patterns are changing very rapidly.

Although the current protocol allowed detection of approximate ‘initial time of enhancement’ in arteries and veins, the temporal resolution was not adequate to resolve the detailed shape of the contrast media bolus. Higher temporal resolution would allow accurate measurement of the arterial input function, speed of propagation of the bolus through vessels feeding the lesion, precise arrival time of the bolus, and extraction and dispersion of the bolus as it passes through the lesion. These parameters may have diagnostic utility.

The very small early signal enhancement detected in ultrafast DCE-MRI data suggests a greatly simplified quantitative approach to data analysis. Linear approximations can be used to calculate small changes in concentration of contrast media as a function of time using a

reference tissue approach (34), and a simplified kinetic model, analogous to a Patlak approach (35), assuming unidirectional flow of contrast media (from capillaries to the extracellular extravascular space), can be used to calculate K^{trans}. This avoids systematic errors due to use of the two compartment model, which may not be appropriate in the breast (36).

This study was performed on a 3 T scanner, while the majority of clinical scans in the United States are performed at 1.5 T (37). A similar protocol has been implemented on a 1.5 T scanner with somewhat lower temporal resolution and good image quality. Since the completion of this pilot study, the protocol described here has been adopted as the clinical protocol at our institution (at both 1.5 T and 3 T), this will allow us to test the kinetic parameters presented here, and other parameters, in a larger dataset; making it possible to identify the parameter, or parameters, that perform the best in a discrimination task. This study and others discussed above have shown several advantages of ultrafast imaging over lower temporal resolution images during the initial uptake phase of breast DCE-MRI.

In conclusion, a protocol for bilateral DCE-MRI breast scans, composed of both high temporal/moderate spatial resolution (ultrafast) scans, and low temporal/high spatial resolution (conventional) scans was tested. The ultrafast images provided new information on early contrast uptake dynamics that could be valuable in classifying breast lesions, while the high spatial resolution images provide the level of detail necessary to evaluate morphology of small lesions. The results from this pilot study suggest that the timing and speed of early signal enhancement could be a valuable marker for malignancy. A larger clinical trial is necessary to assess the sensitivity and specificity of the various parameters introduced here. These results could be obtained with a hybrid protocol that can be easily implemented in a clinical setting, as it relies on standard Fourier sampling methods. Very sparse enhancement during the first 30 – 45 seconds after contrast injection suggests that further acceleration could be obtained with novel acquisition and data processing methods. Detection of small early enhancement may simplify quantitative pharmacokinetic analysis.

Acknowledgements

The authors would like to thank Sharon Harris for her support with recruitment and logistics. This study is supported, in part, by the National Institute of Biomedical Imaging and Bioengineering of the National Institutes of Health under Grant Number T32 EB002103, the National Cancer Institute of the National Institutes of Health under Grant Numbers U01 CA142565; R44 CA186313, R01 CA167785, and R01 CA172801-01, by the European 7th Framework Program grant VPH-PRISM Fp7-ICT-2011-9 and the Segal Family Foundation.

References

1. Turnbull LW. Dynamic contrast-enhanced MRI in the diagnosis and management of breast cancer. NMR Biomed. May.2009 22:28–39. 2007. [PubMed: 18654999]
2. Kuhl CK, Mielcareck P, Klaschik S, et al. Dynamic breast MR imaging: are signal intensity time course data useful for differential diagnosis of enhancing lesions? Radiology. 1999; 211:101–110. Vol. 211; 1999. [PubMed: 10189459]
3. Yankeelov T, Gore J. Dynamic contrast enhanced magnetic resonance imaging in oncology: theory, data acquisition, analysis, and examples. Curr Med Imaging Rev. 2009; 3:91–107. [PubMed: 19829742]

4. Kuhl CK, Schild HH, Morakkabati N. Dynamic bilateral contrast-enhanced MR imaging of the breast: trade-off between spatial and temporal resolution. Radiology. 2005; 236:789–800. [PubMed: 16118161]
5. Tofts PS. Modeling tracer kinetics in dynamic Gd-DTPA MR imaging. J Magn Reson Imaging. 1997; 91:101.
6. Tofts PS, Brix G, Buckley DL, et al. Estimating Kinetic Parameters from Dynamic Contrast-Enhanced T1 -Weighted MRI of a Diffusable Tracer?: Standardized Quantities and Symbols. J Magn Reson Imaging. 1999; 10:223–232. [PubMed: 10508281]
7. Henderson E, Rutt BK, Lee TY. Temporal sampling requirements for the tracer kinetics modeling of breast disease. Magn Reson Imaging. 1998; 16:1057–1073. [PubMed: 9839990]
8. Planey CR, Welch EB, Xu L, et al. Temporal sampling requirements for reference region modeling of DCE-MRI data in human breast cancer. J Magn Reson Imaging. 2009; 30:121–134. [PubMed: 19557727]
9. Jansen SA, Fan X, Medved M, et al. Characterizing early contrast uptake of ductal carcinoma in situ with high temporal resolution dynamic contrast-enhanced MRI of the breast: a pilot study. Phys Med Biol. 2010; 55:N473–N485. [PubMed: 20858914]
10. Pinker K, Grabner G, Bogner W, et al. A combined high temporal and high spatial resolution 3 Tesla MR imaging protocol for the assessment of breast lesions: initial results. Invest Radiol. 2009; 44:553–8. [PubMed: 19652611]
11. Fan X, Medved M, River JN, et al. New Model for Analysis of Dynamic Contrast-Enhanced MRI Data Distinguishes Metastatic from Nonmetastatic Transplanted Rodent Prostate Tumors. Magn Reson Med. 2004; 51:487–494. [PubMed: 15004789]
12. Fan X, Medved M, Karczmar GS, et al. Diagnosis of suspicious breast lesions using an empirical mathematical model for dynamic contrast-enhanced MRI. Magn Reson Imaging. 2007; 25:593–603. [PubMed: 17540270]
13. Jansen SA, Fan X, Karczmar GS, Abe H, Schmidt RA, Newstead GM. Differentiation between benign and malignant breast lesions detected by bilateral dynamic contrast-enhanced MRI: A sensitivity and specificity study. Magn Reson Med. 2008; 59:747–754. [PubMed: 18383287]
14. Evelhoch JL. Key factors in the acquisition of contrast kinetic data for oncology. J Magn Reson Imaging. 1999; 10:254–259. [PubMed: 10508284]
15. DeMartini WB, Liu F, Peacock S, Eby PR, Gutierrez RL, Lehman CD. Background parenchymal enhancement on breast MRI: Impact on diagnostic performance. Am J Roentgenol. Apr.2012 198:373–380.
16. Delille JP, Slanetz PJ, Yeh ED, Kopans DB, Garrido L. Physiologic changes in breast magnetic resonance imaging during the menstrual cycle: Perfusion imaging, signal enhancement, and influence of the T1 relaxation time of breast tissue. Breast J. 2005; 11:236–241. [PubMed: 15982388]
17. Amarosa AR, McKellop J, Klautau Leite AP, et al. Evaluation of the kinetic properties of background parenchymal enhancement throughout the phases of the menstrual cycle. Radiology. 2013; 268:356–65. [PubMed: 23657893]
18. El Khouli RH, Macura KJ, Kamel IR, Jacobs MA, Bluemke DA. 3-T Dynamic Contrast-Enhanced MRI of the Breast: Pharmacokinetic Parameters Versus Conventional Kinetic Curve Analysis. Am J Roentgenol. 2011; 197:1498–1505. [PubMed: 22109308]
19. Mann RM, Mus RD, van Zelst J, Geppert C, Karssemeijer N, Platel B. A Novel Approach to Contrast-Enhanced Breast Magnetic Resonance Imaging for Screening. Invest Radiol. 2014; 49:579–585. [PubMed: 24691143]
20. Platel B, Mus R, Welte T, Karssemeijer N, Mann R. Automated Characterization of Breast Lesions Imaged With an Ultrafast DCE-MR Protocol. IEEE Trans Med Imaging. 2014; 33:225–232. [PubMed: 24058020]
21. Kuhl CK, Schrading S, Strobel K, Schild HH, Hilgers RD, Bieling HB. Abbreviated breast Magnetic Resonance Imaging (MRI): First postcontrast subtracted images and maximum-intensity projection - A novel approach to breast cancer screening with MRI. J Clin Oncol. 2014; 32:2304–2310. [PubMed: 24958821]

22. Petkova M, Gauvrit J-Y, Trystram D, et al. Three-dimensional dynamic time-resolved contrast-enhanced MRA using parallel imaging and a variable rate k-space sampling strategy in intracranial arteriovenous malformations. J Magn Reson Imaging. 2009; 29:7–12. [PubMed: 19097095]
23. Willinek WA, Hadizadeh DR, von Falkenhausen M, et al. 4D time-resolved MR angiography with keyhole (4D-TRAK): more than 60 times accelerated MRA using a combination of CENTRA, keyhole, and SENSE at 3.0T. J Magn Reson Imaging. 2008; 27:1455–60. [PubMed: 18504736]
24. Lim RP, Shapiro M, Wang EY, et al. 3D time-resolved MR angiography (MRA) of the carotid arteries with time-resolved imaging with stochastic trajectories: comparison with 3D contrast-enhanced Bolus-Chase MRA and 3D time-of-flight MRA. AJNR Am J Neuroradiol. 2008; 29:1847–54. [PubMed: 18768727]
25. Song T, Laine AF, Chen Q, et al. Optimal k-space sampling for dynamic contrast-enhanced MRI with an application to MR renography. Magn Reson Med. 2009; 61:1242–8. [PubMed: 19230014]
26. Han S, Paulsen JL, Zhu G, et al. Temporal/spatial resolution improvement of in vivo DCE-MRI with compressed sensing-optimized FLASH. Magn Reson Imaging. 2012; 30:741–52. [PubMed: 22465192]
27. Tudorica, L a.; Oh, KY.; Roy, N., et al. A feasible high spatiotemporal resolution breast DCE-MRI protocol for clinical settings. Magn Reson Imaging. 2012; 30:1257–1267. [PubMed: 22770687]
28. Kershaw LE, Cheng H-LM. A general dual-bolus approach for quantitative DCE-MRI. Magn Reson Imaging. 2011; 29:160–166. [PubMed: 21129878]
29. Ramsay E, Causer P, Hill K, Plewes D. Adaptive bilateral breast MRI using projection reconstruction time-resolved imaging of contrast kinetics. J Magn Reson Imaging. 2006; 24:617–24. [PubMed: 16892204]
30. Wang H, Miao Y, Zhou K, et al. Feasibility of high temporal resolution breast DCE-MRI using compressed sensing theory. Med Phys. 2010; 37:4971–4981. [PubMed: 20964216]
31. Chan RW, Ramsay EA, Cheung EY, Plewes DB. The influence of radial undersampling schemes on compressed sensing reconstruction in breast MRI. Magn Reson Med. 2012; 67:363–77. [PubMed: 21656558]
32. Smith DS, Welch EB, Li X, et al. Quantitative effects of using compressed sensing in dynamic contrast enhanced MRI. Phys Med Biol. 2011; 56:4933–46. [PubMed: 21772079]
33. Chen L, Schabel MC, DiBella EVR. Reconstruction of dynamic contrast enhanced magnetic resonance imaging of the breast with temporal constraints. Magn Reson Imaging. 2010; 28:637–645. [PubMed: 20392585]
34. Medved M, Karczmar G, Yang C, et al. Semiquantitative analysis of dynamic contrast enhanced MRI in cancer patients: Variability and changes in tumor tissue over time. J Magn Reson Imaging. 2004; 20:122–128. [PubMed: 15221817]
35. Patlak CS, Blasberg RG, Fenstermacher JD. Graphical evaluation of blood-to-brain transfer constants from multiple-time uptake data. J Cereb Blood Flow Metab. 1983; 3:1–7. [PubMed: 6822610]
36. Sourbron SP, Buckley DL. On the scope and interpretation of the Tofts models for DCE-MRI. Magn Reson Med. 2011; 66:735–745. [PubMed: 21384424]
37. Bassett LW, Dhaliwal SG, Eradat J, et al. National Trends and Practices in Breast MRI. Am J Roentgenol. 2008; 191:332–339. [PubMed: 18647898]

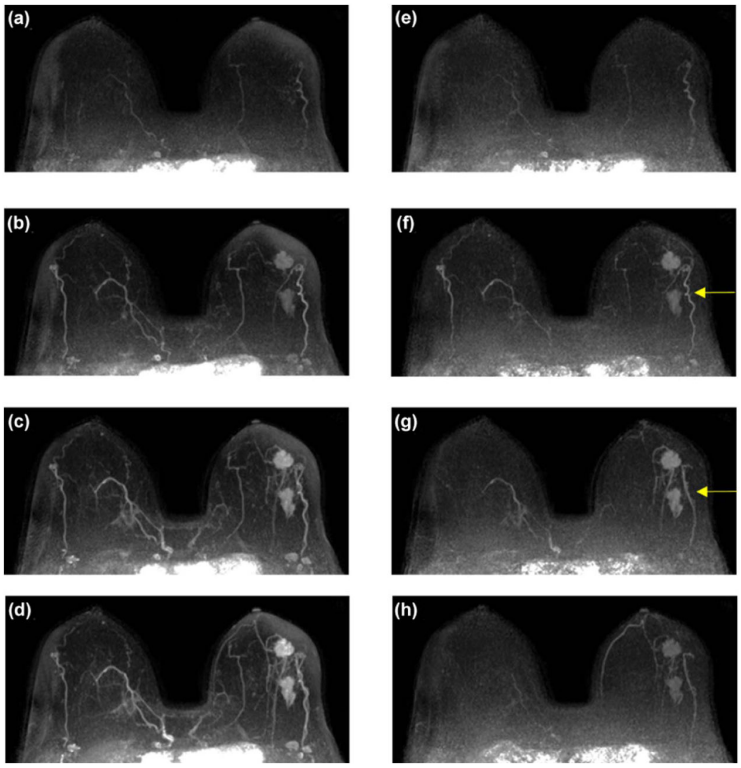

Figure 1.
Maximum intensity projections (MIPs) of ultrafast subtractions (a-d) and enhancement gradient images (e-h). Two invasive ductal carcinomas are visible on image right. Images were acquired with a 9s temporal resolution. Arrows point to vessels feeding and draining a lesion in: (f) arterial phase and (g) venous phase.

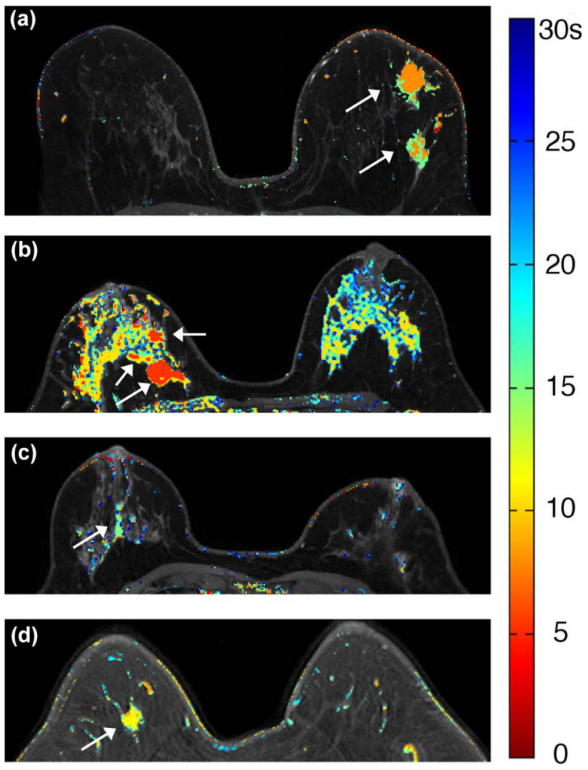

Figure 2.

Examples of time-of-arrival color maps (in seconds) for cases presenting with (lesions marked by arrows): (a) IDC (b) primary and satellite IDC in a case with marked parenchymal enhancement, (c) complex sclerosing lesion and (d) a fibroadenoma. Color scale indicates the time-point at which voxels first began to significantly enhance, relative to time of arrival of the bolus. This image exemplifies the general trend observed, that malignant lesions had shorter TOAs on average.

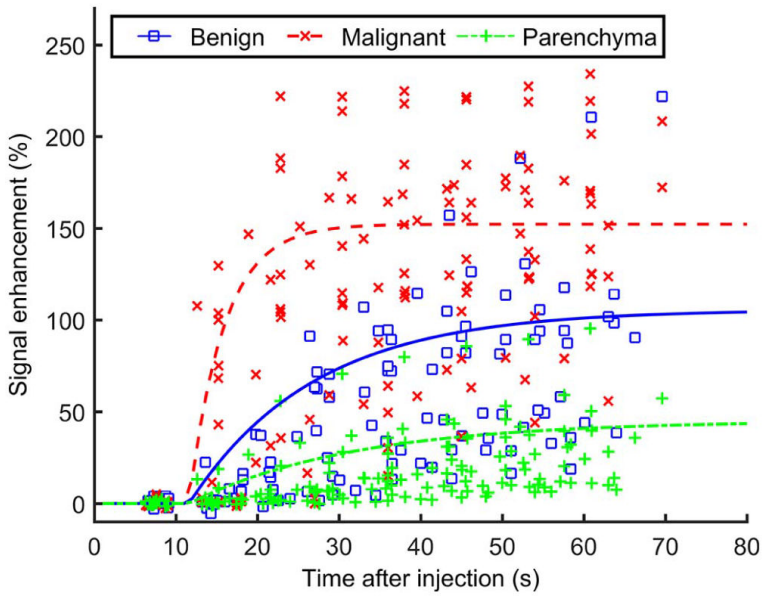

Figure 3.
Scatterplot of average signal enhancement for: malignant lesions, benign lesions and BPE; with their respective average EMM fits.

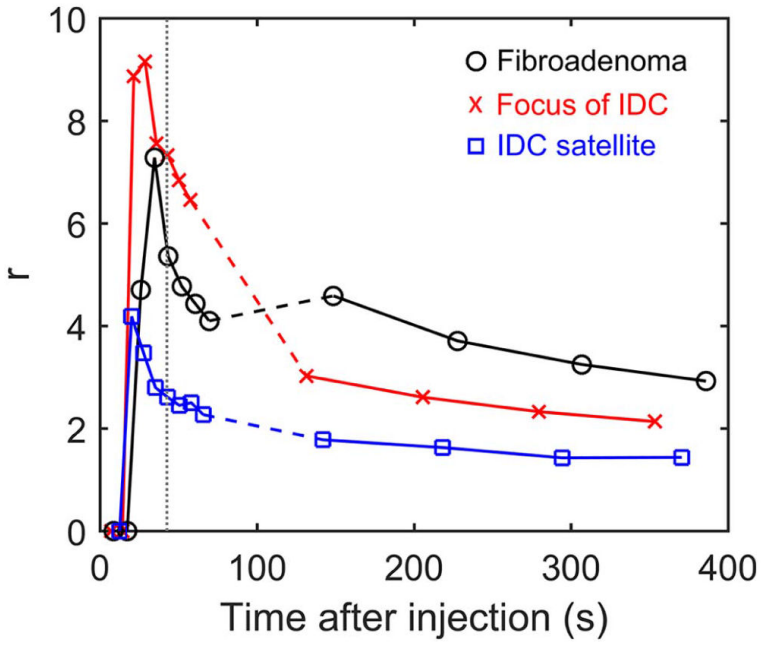

Figure 4.

Plots of the ratio of the signal increase in the lesion to the increase in the background parenchyma for three lesions with marked BPE. The vertical dotted line indicates the approximate time at which the standard clinical protocol would acquire k0. The dashed lines in each curve connect the data points from the ultrafast and standard clinical protocols.

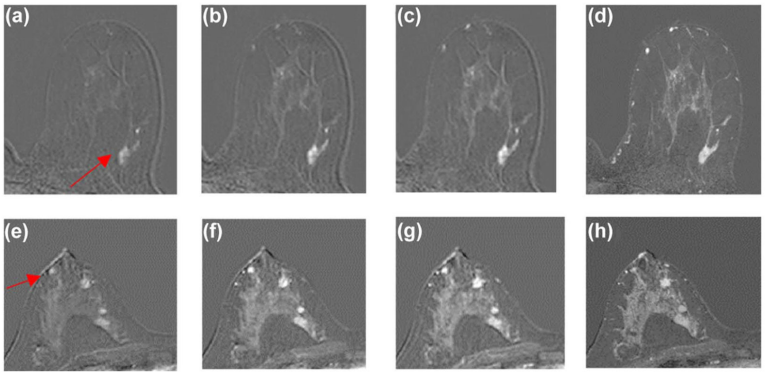

Figure 5.

Two examples of lesions (marked by arrows) where background parenchymal enhancement (BPE) reduces conspicuity in later time-points; (a-c) and (e-g) ultrafast acquisitions; (d) and (h) high spatial resolution images acquired at approximately 2 minutes post-injection. Lesions were: (a-d) a fibroadenoma is visible as an oval circumscribed mass in the early images but is isointense with parenchyma in (d), (e-h) a satellite invasive ductal carcinoma clearly defined in (f) and (g) but is less conspicuous in (h).

Table 1

Acquisition parameters for ultrafast and high spatial resolution sequences

Parameter	Fast	High spatial resolution
TR/TE (ms)	3.2 / 1.6	4.8 / 2.4
Acquisition voxel size (mm^3)	1.5 × 1.5 × 3.0	0.8 × 0.8 × 1.6
SENSE acceleration factor (RL)	4	2.5
SENSE acceleration factor (FH)	2	2
Halfscan (partial Fourier) factor	0.75 (ky); 0.85 (kz)	0.85 (ky); 1 (kz)
Temporal resolution range (s)	6.9 – 9.9	60 – 79.5
Number of slices	100-120	187-225
Flip angle	10°	
Field-of-view (mm)	300 - 370	
Fat suppression method	SPAIR (TR: 155 ms; inversion delay: 80 ms)	

Table 2

Average values (and standard deviations) of kinetic parameters derived from the EMM fits for both benign and malignant lesions and the malignant to benign ratio for the mean value of each parameter.

Parameter	Malignant	Benign	Ratio (M:B)
A (%)	152 ± 48	106 ± 60	1.4
α (%/s) [+]	23 ± 35	6.5 ± 3.3	3.6
Initial Slope [+]	0.42 ± 0.73	0.07 ± 0.05	6.3
iAUC (30s) [+]	33.3 ± 14.3	15.6 ± 10.1	2.5
TOA (s) [+]	6.9 ± 4.6	15.5 ± 13.6	0.4
T90 (s) [+]	27.3 ± 13.9	90.5 ± 139.8	0.3

[+] $p < 0.05$